Drozdenko, D.; Bohlen, J.; Chmelik, F.; Lukac, P.; Dobron, P.:

Acoustic emission study on the activity of slip and twin mechanisms during compression testing of magnesium single crystals

In: Materials Science and Engineering A (2015) Elsevier

DOI: 10.1016/j.msea.2015.10.033

Acoustic emission study on the activity of slip and twin mechanisms during compression testing of magnesium single crystals

Daria Drozdenko[1*], Jan Bohlen[2], František Chmelík[1], Pavel Lukáč[1], Patrik Dobroň[1]

[1]*Charles University in Prague, Department of Physics of Materials, Ke Karlovu 5, 12116, Prague 2, Czech Republic.*

[2]*Helmholtz-Zentrum Geesthacht, Zentrum für Material- und Küstenforschung GmbH, Max-Planck-Straße 1, D21502 Geesthacht, Germany*

*corresponding author: e-mail: drozdenko@karlov.mff.cuni.cz

Abstract

Magnesium single crystals with various crystallographic orientations were uniaxially and channel-die compressed at room temperature (RT) and at a constant strain rate of 10^{-3} s^{-1} in order to obtain a comprehensive set of acoustic emission (AE) data, which can be applied in studies of twinning and dislocation processes in polycrystalline Mg alloys. Loading along the <11.2> axis led to a preferable activation of basal slip and it was accompanied by a low amplitude AE signal. Twinning was exclusively observed during compression along the <10.0> and <11.0> axes. Twin nucleation was characterized by burst AE signals with high amplitudes.

Keywords

Acoustic emission, magnesium, single crystals, dislocation gliding, twinning

1. Introduction

Plastic deformation behavior of magnesium alloys is being intensively studied due to increasing demand for the application of light materials in the automotive and aerospace industry. Magnesium, with the hexagonal close packed (hcp) lattice and the c/a ratio close to the ideal value (1.624), exhibits specific deformation behavior in comparison to materials with cubic lattice due to a limited number of available slip systems at room temperature (RT).

Recently, numerous studies were performed on wrought Mg alloys, which show better mechanical properties in comparison to cast Mg alloys. The deformation behavior of wrought Mg alloys is strongly affected by a crystallographic texture, which is developed during forming or manufacturing processes (extrusion, rolling, forging, etc.) [1, 2].

It is known that plastic deformation in Mg proceeds mainly via activation of four slip systems (basal (00.1) <a>, prismatic (10.0) <a>, pyramidal π1 (10.1) <a>, and pyramidal π2 (11.2) <a+c>) according to their specific critical resolved shear stress (CRSS) [3, 4]. According to the von Mises criterion for a homogeneous deformation of polycrystalline materials at least five independent slip systems are required [5]. In this regard, an additional mechanism, mechanical twinning, is supposed to play an important role to maintain a ductile mechanical behavior of Mg alloys. Twinning modifies the original crystal lattice and the most common twinning mode, {10.2} extension twinning, is characterized by 86 degree misorientation from the original lattice. Twinning itself can accommodate strain to a certain degree. In addition, twins make orientations of the original lattice more favorable for the activation of the dislocation slip, providing additional slip.

Earlier studies [6, 7] have also shown that plastic deformation of Mg and its alloys at RT, besides {10.2} extension twins, could proceed by {10.1} banding, which is a combination of {10.1} twinning followed by {10.2} twinning in the former twin. Basal slip may be subsequently activated in the twinned material and, therefore, can enhance the ability of the material to accommodate strain.

In spite of grain orientation and grain-size effects in polycrystalline wrought materials, plastic deformation is controlled by the same mechanisms as in single crystals. For example, the anisotropy should be similar in strongly textured polycrystals and in single crystals, and the degree of anisotropy should depend on the strength of the texture [6, 8]. This analogy between deformation curves for single crystalline and polycrystalline Mg with a strong texture, giving orientations similar to those of the single crystal, has been observed by Kelley and Hosford [6]. Their study was followed by Graff et al. [9], where mechanical tests and numerical modeling were collated for understanding the mechanisms of dislocation gliding and deformation twinning in single- and polycrystalline Mg. They attempted to describe links between micro- and mesoscale processes. The influence of plane orientation, grain size and temperature on the deformation processes in Mg single crystals was discussed in [6, 10-12].

From all the studies it becomes obvious that the deformation behavior of textured Mg and its alloys can be interpreted in terms of deformation modes observed in single crystals.

The activation of basal and non-basal slip, and twinning in Mg single crystals with different orientations was studied recently [13, 14]. An analysis of the plasticity in Mg single crystals under localized contact using spherical nanoindentation was presented in [15-17]. The finite element simulation [15] indicates for different indentation modes

different spatial locations of the {10.2} extension twins. Crystal plasticity analysis [17] suggests that indentation morphology results from both basal and <a+c> pyramidal slip systems in case of (00.1) indentation and basal and twin systems in case of (1-1.0) and (11.0) indentation. Multiple twinning and dynamic recrystallization during the channel-die compression along the <11.0> direction in c-axis extension at ambient temperature were studied by Molodov et al. [18] with a help of X-ray diffraction, electron backscattered diffraction (EBSD) measurements and theoretical calculations.

Dislocation motion and twinning in metallic materials can be studied using the acoustic emission (AE) phenomenon. The AE technique is based on the detection of transient elastic waves, which are generated by a rapid release of energy due to sudden localized structure changes within the material [19]. During plastic deformation of conventional polycrystalline materials the AE response is characteristic by a distinct peak closed to the yield point, which is followed by a rapid decay of the AE activity [20-21]. The onset AE peak is explained in terms of rapid dislocation multiplication and movement at the beginning of plastic deformation. The subsequent decay of the AE activity is linked with shortening of moving dislocation lines and their flight distance due to increasing density of immobile dislocations.

Thus, it is obvious that each active deformation mechanism will show a specific AE signature. E.g. the activation of multiple slip leading to fast formation of strong barriers to dislocation motion is characteristic as a very rapid decrease of the AE activity [22-24].

The AE signatures belonging to various slip systems and twinning can effectively be studied through plastic deformation of single crystals, where specific conditions can be

controlled by proper orientation of compressive or tensile axis with respect to the single crystal orientation.

Results of AE measurements during mechanical testing on single crystals of various metals (Al, Zn, Fe, Cd, Ti, etc.) can be found e.g. in [19, 25-28]. However, besides [28], we are not aware of any AE studies on Mg single crystals.

The performance of contemporary AE facilities and improved possibilities for analyzing large amounts of data open window for a detailed study on the dynamics of deformation mechanisms in Mg single crystals and the results can be applicable for the interpretation of complex deformation behavior in wrought Mg alloys.

The main aim of the present paper is to obtain a comprehensive set of AE data on uniaxial and plane strain compression tests of Mg single crystals. These data, so far unavailable, will be used as a reference to the results of previous studies of twinning and dislocation processes in polycrystalline Mg alloys with respect to their chemical composition, technological processes and deformation conditions [19-24, 29-32], and for future experiments in this field.

2. Experimental

Mg single crystals of commercial purity (99.95%) were grown by a modified vertical Bridgman technique using specially oriented monocrystalline seeds (c-axis parallel and 45 degree tilted to the growth direction).

The cutting of the specimens (5 x 6 x 10 mm^3) for deformation tests was performed by spark erosion and the quality of specimens was characterized using X-ray diffraction (Panalytical X-ray diffractometer with the CuKα radiation).

Uniaxial and channel-die (Fig. 1) compression tests were performed at RT in universal testing machines Instron 5882 and Zwick Z50 at a constant strain rate of 10^{-3} s^{-1}. The texture after channel-die compression tests of single crystals was determined by X-ray diffraction in order to determine the twinning activity.

Mg single crystalline specimens were uniaxially compressed in four different directions (Fig. 2). Compression along the <11.2> axis gets a set of AE data for crystallographic orientation which specifically favors the basal slip. For other orientations, compression were applied along *c*-, <10.0> and <11.0> axes.

The channel-die compression tests were performed on Mg single crystals in three different crystallographic directions with a suppression of the material flow in the specific direction (Fig. 2b-d). This test was not performed for first orientation (compression along the <11.2> axis), because the constraining to the one flow direction does not exhibit any change in the deformation mechanism (basal slip) and therefore the AE data from the uniaxial compression test are sufficient for the AE analysis.

For next orientation (Fig. 2b), the stress was applied perpendicular to the basal planes with the flow ability in <11.0> direction, i.e. the material flow was constrained in <10.0> direction.

During compression perpendicular to the prismatic (10.0) and (11.0) planes (Fig. 2 c,d) constraint directions were chosen in order to allow material flow in the <00.1> direction.

A computer controlled PCI-2 (Physical Acoustic Corporation) device was used to monitor the AE activity, based on a continuous storage of AE signals with 2 MHz sampling frequency. A miniaturized MST8S (Dakel-ZD Rpety, Czech Republic) piezoelectric transducer with a diameter of 3 mm and flat response in a frequency band

from 100 to 600 kHz was used. The sensor was glued to the holder as close as possible to the specimen. A preamplifier with a gain of 40 dB was used. The full scale of the A/D converter was ±10 V giving the total gain of 100 dB. The background noise during the tests did not exceed 1 mV (~20 dB). With respect to this value, the threshold level of detection was set to 26 dB and a comprehensive set of AE parameters was evaluated.

The following AE parameters were determined:

- AE count rate ($\Delta NC/\Delta t$) - is the count number per time unit [25] at a given threshold voltage level.
- AE event – AE event starts by crossing a defined threshold voltage level and the end of the event is detected when the signal remains below the threshold voltage for a period exceeding a Hit Definition Time (HDT). Afterwards, during a Hit Lockout Time (HLT), the AE signal is not parametrized in order to filter out sound reflections. To separate individual AE events, HDT and HLT were set to 800 and 1000 μs, respectively.
- Peak amplitude of the AE event – the maximum of the AE signal within an individual AE event.

The AE events and their peak amplitudes were determined in order to discriminate low and high amplitude sources of the AE signal.

3. Results

3.1. Uniaxial compression

The stress and the AE signal voltage *vs.* time dependences for uniaxially compressed Mg single crystals are depicted in Fig. 3. The proportionality between time and strain is given by the constant strain rate of $10^{-3}s^{-1}$. For the specimen with a favorable orientation

for basal slip (compression along the <11.2> axis, Fig. 3a) the stress is accumulated very slowly and the stress-time curve exhibits a very long stage I (easy glide). During uniaxial compression along the c-axis, Fig. 3b, a strong hardening behavior (stage II) occurs already at the very beginning of the test.

The deformation curves for compression along the <10.0> and <11.0> axes (Fig. 3c,d) exhibit a relative long stage I, where a more distinct stress increase was observed for compression along the <11.0> axis.

The AE count rate and the peak amplitudes of the AE events, as basic AE parameters, are correlated with the deformation curves and presented in Fig. 4. Compression of Mg single crystal along the <11.2> axis is accompanied by a relatively weak AE signal at the beginning of plastic deformation. Fig. 4a shows that the AE count rate is relatively constant during the test. During compressing along the *c*-axis, a low AE activity is observed during the whole test (Figs. 3b, 4b).

For compressed Mg single crystals along the <10.0> and <11.0> axes, both AE parameters exhibit their maxima at the beginning of plastic deformation. The AE signal voltage (Fig. 3c,d), as well as the AE count rate, is higher (by factor of approx. 6, Fig. 4c,d) during compression along the <11.0> axis than during that along the <10.0> axis. Moreover, larger amount of AE events with higher peak amplitudes can be seen in Fig. 4d by comparison to Fig. 4c.

3.2. Channel-die compression

During channel-die compression along the *c*-axis, plastic deformation proceeds in a similar way as during uniaxial compression. The rapid increase in stress is evident from the very beginning of the test. A small amount of AE events was observed at the

beginning of the test. Shortly before fracture, the AE signal was emitted by crack propagation. Therefore, deformation curve with a concurrent AE measurement is not plotted here.

The experimental data from mechanical testing with concurrent AE measurement for channel-die compressed Mg single crystals along the <10.0> and <11.0> axes are presented in Fig. 5 and Fig. 6. The deformation curves exhibit a relative long stage I with a low work hardening. This work hardening is slightly higher for loading along the <11.0> axis than along the <10.0> axis.

For both orientations, the AE signal shows a burst character with high amplitudes, whereas for the compression along the <11.0> axis, the AE signal is weaker (Fig. 5).

The AE count rates in both cases exhibit a maximum at the beginning of plastic deformation, which is followed by its slow decrease (Fig. 6). Higher values of AE count rate are observed during whole test for the compression along the <11.0> axis by comparison to compression along the <10.0> axis.

To reveal possible twinning activity during channel-die compression, the texture measurements of the single crystals before and after loading were performed and the results can be found in Fig. 7. The texture of the single crystal prior to deformation (Fig. 7a,c) was characterized by very high intensity peaks corresponding to the orientation ($\varphi 1$, Φ, $\varphi 2$) = (90°, 45°, 30°) and (90°, 90°, 30°) in Euler space (Bunge notation) for compression of Mg single crystals in orientations presented in Fig. 2c,d, respectively.

The texture of the specimen, compressed along the <10.0> axis, is composed of an initial component (90, 45, 30), two symmetrical components (225, 45, 30) and (300, 45, 30), and further two weak components (marked in the Fig. 7b as zone 1 and 2,

respectively). Two symmetrical components duplicate intensity peaks in the (10.0) pole figure of the initial texture. It is worth noting that the weak intensity peaks which correspond to the initial orientation (90, 45, 30) were slightly rotated, and therefore did not match the exact orientation (90, 45, 30) as for the initial state (Fig. 7a).

The texture of the specimen after compression along the <11.0> axis consists of an initial component and two new symmetrical texture components (0, 30, 30) and (180, 30, 30) with an angle of 30° between the direction of their respective c-axes and the compression axis (Fig. 7d). The weak intensity peaks, which correspond to the initial orientation, were slightly rotated around compression axis and as in previous case they did not match the exact orientation. Moreover, the textures after compression became asymmetrical in terms of their relative intensity in the (00.2) and (10.0) pole figures.

4. Discussion

The main difference between the uniaxial and the channel-die compression tests is the direction of plastic flow of the material. Basically, in the case of uniaxial compression along a loading axis, the material flow is perpendicular to the loading direction without constraint. In case of the channel-die tests, see Fig. 1 again for visualization, the plastic deformation is realized in one direction only and in one direction the material flow is restricted (in our case applies for the (11.0) and (10.0) planes). Through this experiment specific deformation mechanisms can be restricted.

4.1. Uniaxial compression of single crystal along the <11.2> axis: basal slip

A Schmid factor (SF) analysis [8] reveals that compression of single crystal along the <11.2> axis (45 degree tilted *c*-axis from loading direction) is the ideal condition for the

activation of basal slip. Other types of dislocation slip are less engaged in the stage I of the deformation due to higher CRSS [3, 4, 6, 7, 33]. Therefore, the AE activity can be related to the basal slip. From these results, it can be clearly seen that collective movement of dislocations in single slip mode produce low amplitude AE signal.

4.2. Uniaxial compression of single crystal along the c-axis: pyramidal slip

In case of compression along the *c*-axis (Fig. 2b), SF for the basal, prismatic and pyramidal π1 {10.1} slip systems are zero [8]. Furthermore, it was shown that the {10.2} twinning system is also not activated [8, 29, 34]. The 6 equivalent pyramidal π2 slip systems are active and considering cross-slip of <c+a> dislocation onto {2-1.2} and {10.1} planes, 12 slip systems are available to accommodate plastic deformation. A very strong hardening is observed due to the intersection of the slip planes [8]. This type of dislocation slip was identified by the TEM measurements in earlier works [35, 36]. Studies of the evolution of the relative activities of various slip systems with increasing strain [9], also show prevailing pyramidal <c+a> slip.

The very low AE activity (Fig. 4b) during the whole test is consistent with a rapid immobilization of dislocations due to a formation of strong obstacles.

4.3. Uniaxial compression of single crystals along the <10.0> and <11.0> axes: twinning and dislocation glide

Plastic deformation in the crystal during compression along the <10.0> and <11.0> axes is accommodated mainly by prismatic slip and twinning. For compression along the <10.0> axis, SF for prismatic (0.43) and basal (0) slips, and extension twinning system (0.5) was calculated in [8]. Analogous calculation of SF for compression along <11.0>

axis for prismatic (0.43) and basal (0) slips, and extension twinning system (0.37) are presented in [8] as well. The activation of individual deformation mechanism depends on both SF and CRSS (the best combination is high SF and low CRSS). The CRSS for the prismatic slip is higher than the activation stress for twinning. Consequently, the plastic deformation during compression along the <10.0> and <11.0> axes proceeds first of all by twinning giving a stronger hardening by comparison with the basal slip activated during compression along the <11.2> axis [6-9].

In Mg, {10.2}<10.-1> twins can accommodate the extension up to 6.4% along the *c*-axis [37]. Furthermore, reorientation of basal planes due to the extension twinning (rotation of basal planes by 86.3 degrees with respect to their original orientation [10]) promotes additional plastic deformation produced by easier basal slip in the reoriented grains. It was shown by electron backscatter diffraction (EBSD) mapping [12, 17, 18] and TEM investigation [15, 16] that twins are mainly nucleated at the beginning of the compression along the <10.0> and <11.0> axes.

The calculation of the SF for extension twinning [29] with respect to loading direction shows that 6 variants of twinning are possible during compression along the <10.0> axis. Two of them with SF = 0.5 and four variants with SF = 0.15. In the case of compression along the <11.0> axis, only four variants of twinning having SF = 0.35 can be active with the same probability. Thus, higher twinning activity at the beginning of plastic deformation gives a higher flow stress (more pronounced hardening) and extended stage I during compression along the <11.0> axis than along the <10.0> axis.

Hence, it can be concluded that during compression along the <10.0> and <11.0> axes, the AE originates from extension twins. In earlier works [27, 38] it was reported that the

twin nucleation produces a detectable AE in contrary to the twin growth. Thus, the high amplitude AE signal can be associated with a twin nucleation.

The difference during loading along the <10.0> and <11.0> axes, i.e. the rotation of crystal along the *c*-axis by 30 degrees, is clearly reflected in the AE response. Higher twinning activity during compression along the <11.0> axis is consistent with a higher AE response (Fig. 4) for this orientation. It confirms that in this orientation four variants of extension twins with SF of 0.35 are more likely to be activated than two variants with the higher SF in case of compression along the <10.0> axis. It should be noted that minor part of the AE response could be produced by additional basal slip in reoriented crystal planes similar to compression along the <11.2> axis, see section 4.1.

The activation of additional (non-basal) slip systems with higher CRSS is clearly manifested as a strong increase in the engineering stress (stage II on deformation curve) for both orientations (Figs. 3,4 c,d). The dislocation density increases with a progress of plastic deformation, what leads to a decrease in the free path of moving dislocations and therefore a reduction of the AE activity is observed (similar situation as in the stage II during compression along the *c*-axis).

4.4. Channel-die compression in the orientation 2: pyramidal slip

The deformation behavior during both uniaxial (Fig. 2b) and channel-die compression (not presented here) along the *c*-axis is similar. A very strong hardening is the result of the activation of the pyramidal $\pi 2$ slip systems and a possible cross-slip of <c+a> dislocations. The very low AE activity during the whole test can be ascribed to a fast formation of immobile dislocations. Therefore, we can summarize that constraining of

the (10.0) planes has practically no influence on plastic deformation during compression along the *c*-axis.

4.5. Channel-die compression during compression along the <10.0> and <11.0> axes: "restricted" twinning and dislocation glide

During channel-die compression along the <10.0> and <11.0> axes, active twin variants are influenced by constraining of (11.0) and (10.0) planes, respectively, leading to a change in the deformation behavior by comparison to uniaxial compression test. The deformation curves for channel-die compression tests are similar to those presented by Kelley and Hosford [7]. As for the uniaxial compression, the hardening in stage I is higher during compression along the <11.0> axis than along the <10.0> axis. It was shown in [17, 18] that the early stage of deformation during channel-die compression along the <10.0> and <11.0> axes was characterized by large scale {10.2} extension twinning, converting the whole specimen into softer orientation for slip.

The texture intensity peak, which corresponds to the initial orientation, was slightly rotated around compression axis during loading along the <10.0> axis (Fig. 7a,b). This behavior could be explained by dislocation slip in areas of single crystals, which were not twinned till the end of the test [18].

The texture components formed during loading in both orientations can be ascribed to the result of extension twinning. The asymmetrical character of texture components originated from twins could be related to dislocation gliding in reoriented material [18].

An illustration of active twinning systems, which is based on the results of texture measurements after channel-die compression of Mg single crystal, is presented in Fig. 8. For specimen compressed along the <10.0> axis twin variants with SF of 0.15 are

depicted as twin A, B and twin variant with SF of 0.5 is shown as twin C. Small component in the texture, marked as zone 1 in Fig. 7b, results from activation of twin C, however this deformation mode is not preferred due to the configuration of the test. Thus, it can be assumed that twins have a tendency to retwin into orientation for easy material flow. Consequently, a small texture component, marked as zone 2 in Fig. 7b, could be associated with double twin from twin C (detail in the Fig. 8a). For specimen compressed along the <11.0> axis extension twin variants with SF of 0.35 are depicted as twins A and B, respectively.

The higher AE response during compression along the <11.0> axis than along the <10.0> axis is ascribed to higher twinning activity (Fig. 6), similarly to uniaxial compression test. Thus, during channel-die test four variants of extension twins with SF of 0.35 have higher influence on plastic deformation than two variants with higher SF (0.5). The numerical simulations and experimental results show analogous mechanical behavior [8, 9].

During compression along the <10.0> axis the peak amplitudes of AE events at the stage I of the deformation curve are higher for channel-die compression than for uniaxial test (Fig. 4a, 6a). According to [38], this behavior could be attributed to a high twin nucleation. Therefore, we can conclude that constraining of (11.0) plains restricts grown of extension twins and extension along the *c*-axis is accommodated mainly by increase of number of nucleated twins rather than by their grown.

Similar to uniaxial compression, during channel-die compression the activation of non-basal slip systems is associated with a strong decrease in the AE activity due to a fast immobilization of dislocations.

Conclusions

Mg single crystals with different orientation were subjected to uniaxial and channel-die compression tests with a concurrent recording of acoustic emission (AE). The active deformation mechanisms were correlated to the AE response. Loading along the <11.2> axis led to a dominant activity of basal <a> slip and AE is represented by a low amplitude AE signal. During uniaxial and channel-die compression along the *c*-axis, pyramidal $\pi 2$ slip systems were activated, and due to a rapid immobilization of dislocations a formation of strong obstacles, a very weak AE signal was observed for both arrangement of deformation tests. The higher twinning activity, represented by a more pronounced AE response, was observed during uniaxial compression along the <11.0> than the <10.0> axes. A minor part of the AE response could be produced by additional basal slip in reoriented crystal planes. Similar deformation behavior is observed for channel-die compression, where constraining of specific planes led to higher amount of twins and it is reflected in higher AE by comparison to the uniaxial compression.

Acknowledgements

This work received support by the Czech Science Foundation under the 13 - 19812S, by the Grant Agency of Charles University under the grant 1882314 and also by the grant SVV-2015- 260213. The work of P.D. is a part of activities of the Charles University Research Center "Physics of Condensed Matter and Functional Materials".

References

[1] W.F. Hosford, R.M. Caddell, Metal forming: mechanics and metallurgy, second ed., PTR Prentice Hall: Upper Saddle River, NJ, 1993.

[2] K.U.Kainer (ed.), Magnesium Alloys and Technologies, Cambridge: Wiley-VCH, Weinheim, 2003.

[3] S. Ando, H. Tonda, Non-basal Slip in Magnesium and Magnesium-Lithium Alloy Single Crystals, Mater. Sci. Forum 350-351 (2000) 43-48.

[4] A. Staroselsky, L. Anand, A constitutive model for hcp materials deforming by slip and twinning: application to magnesium alloy AZ31B, Int. J. Plasticity 19 (10) (2003) 1843-1864.

[5] R.Von Mises, Mechanik der plastischen Formanderung von Kristallen, Z. Angew. Math. Mech. 8 (1928) 161-185.

[6] E.W. Kelley, W.F. Hosford, Plane-strain compression of Magnesium and Magnesium Alloy Crystals, Trans. Metall. Soc. AIME 242 (1968) 5–13.

[7] E.W. Kelley, W.F. Hosford, The deformation characteristics of textured magnesium, Trans. Metall. Soc. AIME 242 (1968) 654 - 661.

[8] G.S.Kim, Small volume investigation of slip and twinning in magnesium single crystals, PhDthesis, 2011.

[9] S. Graff, W.Brocks, D.Steglich, Yielding of magnesium: from single crystal to polycrystalline aggregates, Int. J. Plasticity 23 (2007) 1957-1978.

[10] B.C. Wonsiewicz and W.A. Backofen, Plasticity of Magnesium Crystals, Trans. TMS-AIME 239 (1967) 1422–1431.

[11] P.W. Bakarian, C.H. Mathewson, Slip and twinning of magnesium single crystals at elevated temperatures, Trans. AIME 152 (1943) 226.

[12] A. Chapuis, J.H. Driver, Temperature dependency of slip and twinning in plane strain compressed magnesium single crystals, Acta Mater. 59 (5) (2011) 1986-1994.

[13] B. Sulkowski, Analysis of Crystallographic Orientation Changes during deformation of magnesium sungle crystals, Acta Phys. Pol. A 126 (3) (2014) 768-771.

[14] F. Hiura and M. Niewczas, Latent hardening effect under self- and coplanar dislocation interactions in Mg single crystals, Scripta Mater. 106 (2015) 17-20.

[15] B Selvarajou, J-H. Shin, T.K. Ha, I. Choi, S.P. Joshi, H.N. Han, Orientation-dependent indentation response of magnesium single crystals: Modeling and experiments, Acta Mater. 81 (2014) 358–376.

[16] D. Catoor, Y.F. Gao, J. Geng, M.J.N.V. Prasad, E.G. Herbert, K.S. Kumar, G.M. Pharr, E.P. George, Incipient plasticity and deformation mechanisms in single-crystal Mg during spherical nanoindentation, Acta Mater. 61 (8) (2013) 2953–2965.

[17] H. Kitahara, T. Mayama, K. Okumura, Y. Tadano, M. Tsushida, S. Ando, Anisotropic deformation induced by spherical indentation of pure Mg single crystals, Acta Mater. 78 (2014) 290–300.

[18] K.D. Molodov, T. Al-Samman, D.A. Molodov, G. Gottstein, Mechanisms of exceptional ductility of magnesium single crystal during deformation at room temperature: Multiple twinning and dynamic recrystallization, Acta Mater. 76 (2014) 314–330.

[19] C.R. Heiple and S.H. Carpenter, Acoustic Emission Produced by Deformation of Metals and Alloys - A Review: Part I, J. Acoustic Emission 6 (1987) 177-204.

[20] P. Dobroň, J. Bohlen, F. Chmelík, P. Lukáč, D. Letzig, K.U. Kainer, Mechanical anisotropy of AZ31 magnesium alloy sheet investigated by the acoustic emission technique, Kovove Mater. 45 (3) (2007) 129-133.

[21] O. Muránsky, M.R. Barnett, D.G. Carr, S.C. Vogel, E.C. Oliver, Investigation of deformation twinning in a fine-grained and coarse-grained ZM20 Mg alloy: Combined in situ neutron diffraction and acoustic emission, Acta Mater. 58 (5) (2010) 1503–1517.

[22] F. Chmelík, E. Pink, J. Król, J. Balík, J. Pešička, P. Lukáč, Mechanisms of serrated flow in aluminium alloys with precipitates investigated by acoustic emission, Acta Mater. 46 (12) (1998) 4435–4442.

[23] D.R. James, S.H. Carpenter, The effect of sample size on the acoustic emission generated during tensile deformation of 7075 aluminum alloy, Scripta Metall. 10 (8) (1976) 779–781.

[24] M. Lugo, J.B. Jordon, M.F. Horstemeyer, M.A. Tschopp, J. Harris, A.M. Gokhale, Quantification of damage evolution in a 7075 aluminum alloy using an acoustic emission technique, Mat. Sci. Eng. A 528 (22–23) (2011) 6708–6714.

[25] ASTM E750-04 Standard Practice for Characterizing Acoustic Emission Instrumentation, Book of Standards Volume 03.03, ASTM Inernational (2004).

[26] T. Richeton, P. Dobroň, F. Chmelík, J. Weiss, F. Louchet, On the Critical Character of Plasticity in Metallic Single Crystals, Mat. Sci. Eng. A 424 (2006) 190–195.

[27] C.R. Heiple and S.H. Carpenter, Acoustic Emission Produced by Deformation of Metals and Alloys – A review: Part II., J. Acoustic Emission 6 (1987) 215-237.

[28] R.M. Fisher and J.S. Lally, Microplasticity detected by an acoustic technique, Can. J. Physics 45 (1967) 1147-1159.

[29] J.Čapek, K.Máthis, B.Clausen, J.Stráská, P.Beran, P.Lukáč, Study of the loading mode dependence of the twinning in random textured cast magnesium by acoustic emission and neutron diffraction methods, Mat. Sci. Eng. A 602 (2014) 25-32.

[30] E. Meza-García, P. Dobroň, J. Bohlen, D. Letzig, F. Chmelík, P. Lukáč, K.U. Kainer, Deformation mechanisms in an AZ31 cast magnesium alloy as investigated by the acoustic emission technique, Mat. Sci. Eng. A 462 (1–2) (2007) 297-301.

[31] P. Dobroň, J.Balík, F. Chmelík, K.Illková, J. Bohlen, D. Letzig, A study of mechanical anisotropy of Mg–Zn–Rare earth alloy sheet, J. Alloys Comp. 588 (2014) 628-632.

[32] A. Vinogradov, D. Orlov, A. Danyuk, Y. Estrin, Deformation mechanisms underlying tension–compression asymmetry in magnesium alloy ZK60 revealed by acoustic emission monitoring, Mat. Sci. Eng. A 621 (2015) 243–251.

[33] H.L. Kim, J.S. Park, Y.W. Chang, Effects of lattice parameter changes on critical resolved shear stress and mechanical properties of magnesium binary single crystals, Mat. Sci. Eng. A 540 (2012) 198–206.

[34] P.G. Partridge, The crystallography and deformation modes of hexagonal close-packed metals, Metall. Rev. 12 (1967) 169-194.

[35] T. Obara, H. Yoshinaga, S. Morozumi, {11-22}<-1-123> slip system in magnesium, Acta Metall. 21 (1973) 845-853.

[36] J.F. Stohr, J.P. Poirier, Etude en Microscopie Electronique de Glissement Pyramidal {1122}<1123> dans le Magnesium, Phil. Mag. 25 (1972) 1313-1329.

[37] U.F. Kocks, D.G. Westlake, The important of twinning for the ductility of CPH polycrystals, Trans. Metall. Soc. AIME 239 (1967) 1107-1109.

[38] J.P. Toronchuk, Acoustic emission during twinning of zinc single crystals, Mater. Eval. (1977) 51-53.

List of figure captions:

Fig. 1. Scheme of channel-die compression experiment.

Fig. 2. Orientations of Mg single crystals for selection of compression axes; flow axis is marked for channel-die experiment.

Fig. 3. Time dependence of engineering stress and the AE signal voltage for Mg single crystals with respect to various loading axes (uniaxial compression): (a) <11.2>, (b) *c*-, (c) <10.0>, (d) <11.0>.

Fig. 4. Time dependences of engineering stress, the AE count rate, and the peak amplitudes of the AE events for Mg single crystals with respect to various loading axes (uniaxial compression): (a) <11.2>, (b) *c*-, (c) <10.0>, (d) <11.0>.

Fig. 5. Time dependences of engineering stress and AE signal for Mg single crystals with respect to various loading axes (channel-die compression): (a) <10.0>, (b) <11.0>.

Fig. 6 Time dependences of the engineering stress, the AE count rate, and the peak amplitudes of the AE events for Mg single crystals with respect to various loading axes (channel-die compression): (a) <10.0>, (b) <11.0>.

Fig. 7. Texture development in the single crystals for channel-die compression along the <10.0> and <11.0> axes prior to (a, c) and after (b, d, respectively) loading.

Fig. 8. Illustration of active twinning system in the Mg single crystal during channel-die compression along the <10.0> (a) and <11.0> (b) axes. In detail of (a) double twinning of original lattice (Matrix=M.) is presented.

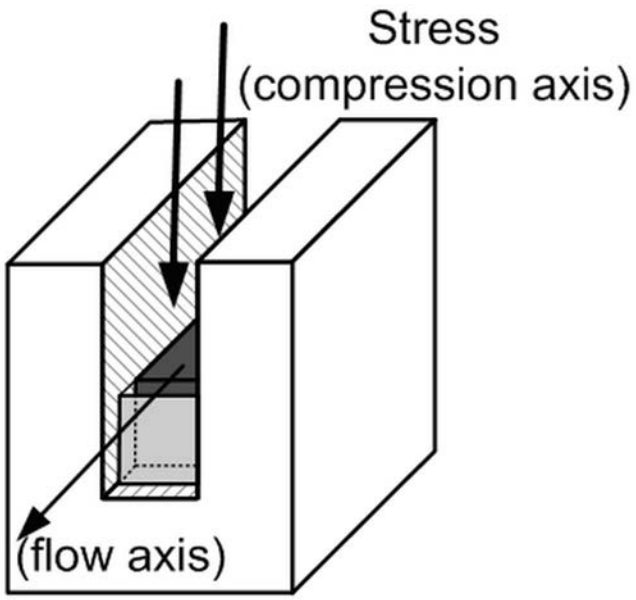

Fig. 1. Scheme of channel-die compression experiment.

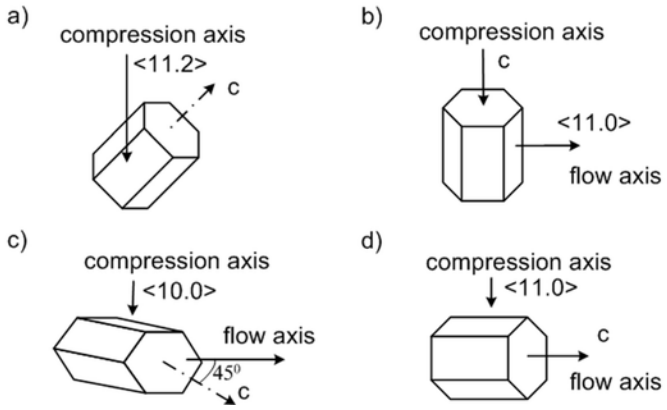

Fig. 2. Orientations of Mg single crystals for selection of compression axes; flow axis is marked for channel-die experiment.

a)

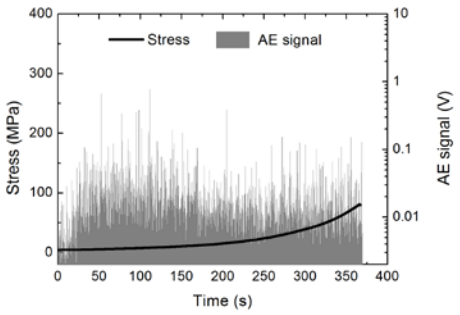
Stress
AE signal
Stress (MPa)
AE signal (V)
Time (s)
0
100
200
300
400
0.01
0.1
1
10
0
50
100
150
200
250
300
350
400

b)

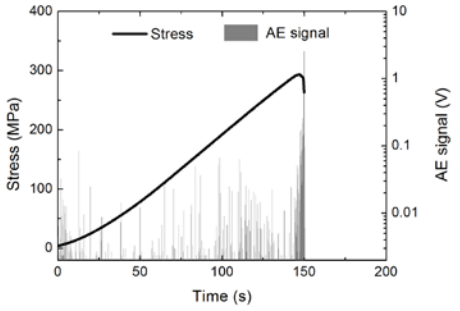
Stress
AE signal
Stress (MPa)
AE signal (V)
Time (s)
0
100
200
300
400
0.01
0.1
1
10
0
50
100
150
200

c)

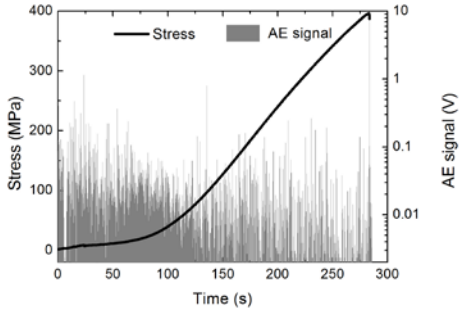
Stress
AE signal
Stress (MPa)
AE signal (V)
Time (s)
0
100
200
300
400
0.01
0.1
1
10
0
50
100
150
200
250
300

d)

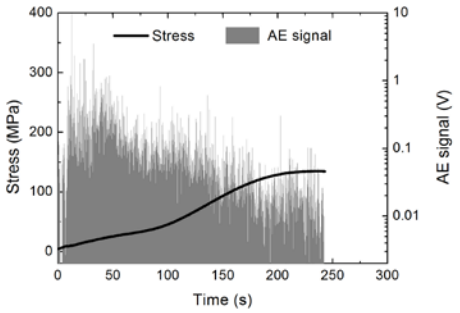
Stress
AE signal
Stress (MPa)
AE signal (V)
Time (s)
0
100
200
300
400
0.01
0.1
1
10
0
50
100
150
200
250
300

Fig. 3. Time dependence of engineering stress and the AE signal voltage for Mg single crystals with respect to various loading axes (uniaxial compression): (a) <11.2>, (b) *c*-, (c) <10.0>, (d) <11.0>.

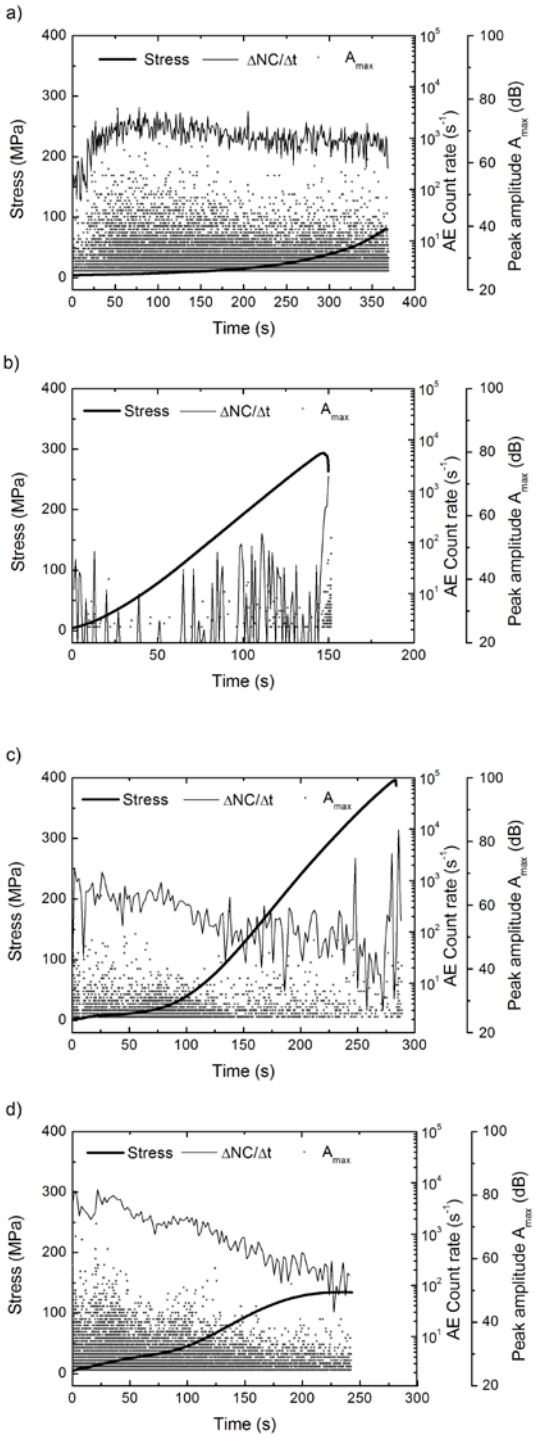

Fig. 4. Time dependences of engineering stress, the AE count rate, and the peak amplitudes of the AE events for Mg single crystals with respect to various loading axes (uniaxial compression): (a) <11.2>, (b) *c*-, (c) <10.0>, (d) <11.0>.

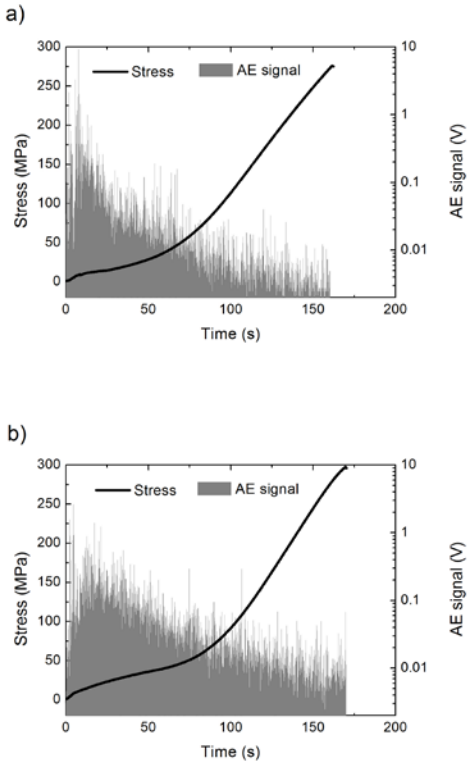

Fig. 5. Time dependences of engineering stress and AE signal for Mg single crystals with respect to various loading axes (channel-die compression): (a) <10.0>, (b) <11.0>.

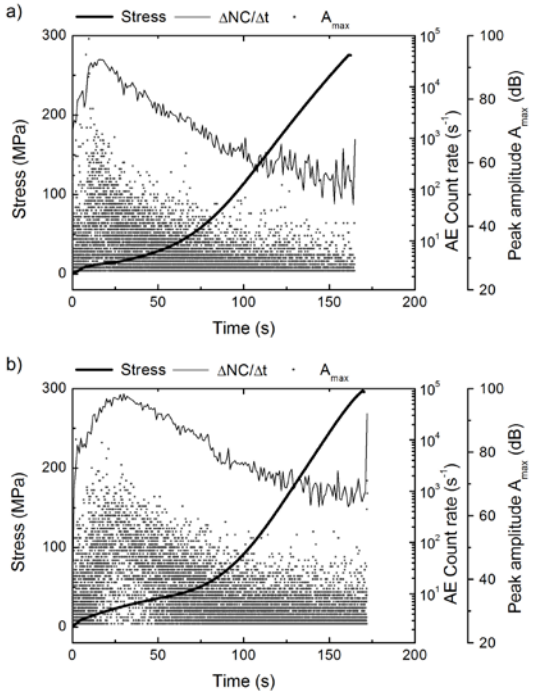

Fig. 6 Time dependences of the engineering stress, the AE count rate, and the peak amplitudes of the AE events for Mg single crystals with respect to various loading axes (channel-die compression): (a) <10.0>, (b) <11.0>.

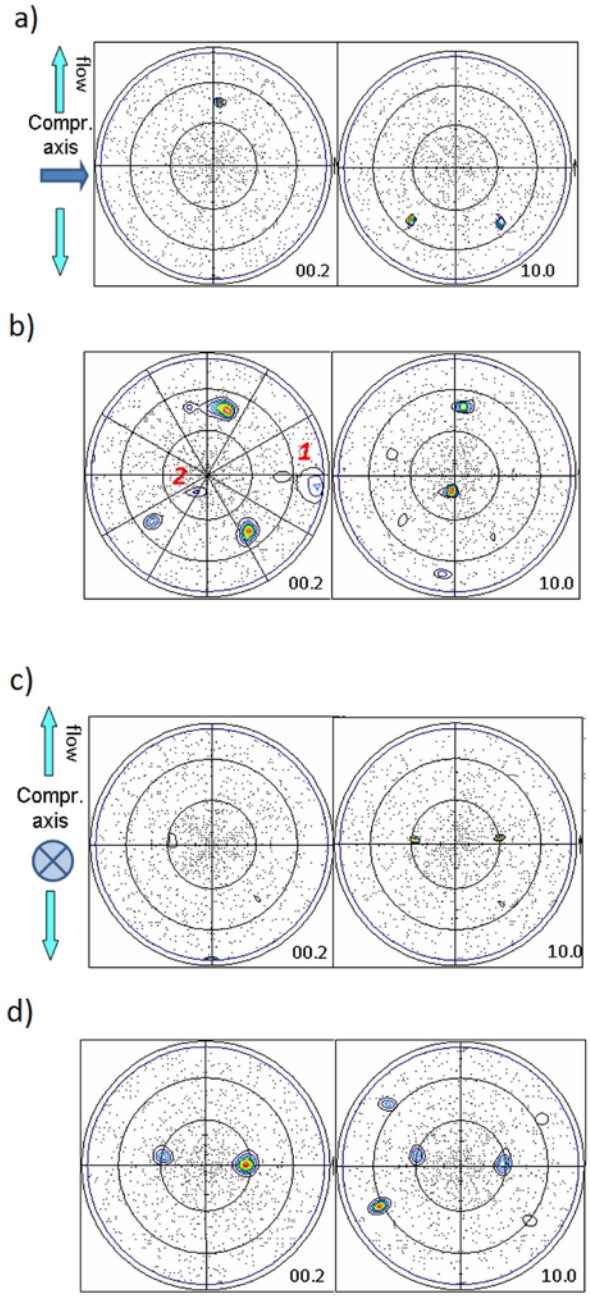

Fig. 7. Texture development in the single crystals for channel-die compression along the <10.0> and <11.0> axes prior to (a, c) and after (b, d, respectively) loading.

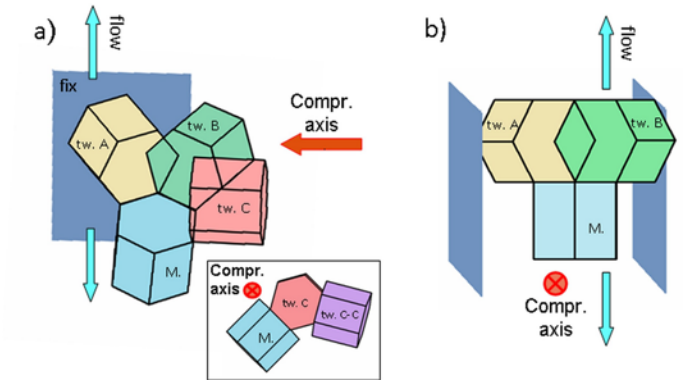

Fig. 8. Illustration of active twinning system in the Mg single crystal during channel-die compression along the <10.0> (a) and <11.0> (b) axes. In detail of (a) double twinning of original lattice (Matrix=M.) is presented.